Enolase-1 is essential for neutrophil recruitment during acute inflammation

Hseuh-Yen Lu[1], Ping-Hsiang Huang[1,4], Ting-Wei Lee[2,4], Hui-Wen Chang[2], Nai-Yu Chen[1], Yu-Jing Zhuang[1], Ta-Tung Yuan[3], and Chun-Jen Chen[1,5]*

[1]Department of Biochemical Science and Technology, National Taiwan University, Taipei 106319, Taiwan (R.O.C.)

[2]Graduate Institute of Molecular and Comparative Pathobiology, School of Veterinary Medicine, National Taiwan University, Taipei 106319, Taiwan (R.O.C.)

[3]HuniLife Biotechnology Inc., Taipei 114, Taiwan (R.O.C.)

[4]These authors contributed equally

[5]Lead contact

*Correspondence: cjchen1@ntu.edu.tw

Summary

Enolase-1 (ENO1) is a ‘moonlighting protein’ with multiple functions. When expressed on the cell surface, ENO1 binds plasminogen (PLG) and facilitates cell migration via plasmin (PLM)-mediated lysis of extracellular matrix proteins. Here, we observed that ENO1 expression on the neutrophil surface was markedly increased upon inflammatory stimulation both in vitro and in vivo. An anti-ENO1 monoclonal antibody (mAb), 7E5, which blocks ENO1-PLG interaction, effectively suppressed the fibrinolytic activity of inflammatory neutrophils. In mouse models of acute inflammation, including lipopolysaccharide (LPS)-induced lung injury and necrotic cell challenge, the 7E5 mAb significantly reduced neutrophil recruitment and the formation of neutrophil extracellular traps (NETs). Furthermore, 7E5 neutralized the immunostimulatory activity of soluble ENO1 protein, which was substantially elevated in the circulation of animals during acute inflammation. These findings suggest that ENO1 plays a crucial role in triggering inflammation and mediating neutrophil infiltration. Targeting ENO1 using antibodies could represent a promising strategy to mitigate tissue damage caused by excessive neutrophilic inflammation.

Introduction

Neutrophils are the first innate immune cells recruited from the bloodstream to sites of microbial infection or tissue injury during acute inflammation. These cells efficiently kill invading pathogens through mechanisms such as phagocytosis, the release of granular enzymes and reactive oxygen species (ROS), and the formation of neutrophil extracellular traps (NETs) [1]. Additionally, neutrophils produce cytokines and chemokines that modulate the function of other leukocytes [2]. However, these antimicrobial mechanisms are inherently cytotoxic and may cause collateral damage to host tissues during inappropriate or excessive inflammation. This can lead to pathogenic autoimmunity or chronic inflammation [3-5]. In the context of acute respiratory distress syndrome (ARDS) associated with the COVID-19 pandemic, infection with severe acute respiratory syndrome coronavirus 2 (SARS-CoV-2) can trigger robust neutrophil recruitment and activation. This process may contribute to lung damage, cytokine storm, septic shock, and even multiple organ failure [6,7].

In response to infection or injury, neutrophils migrate from the bloodstream to sites of insult via a complex multistep cascade. Cytokines and chemokines produced by tissue-resident innate immune cells stimulate neutrophils to express adhesion molecules, such as integrins and selections, which interact with counter-receptors expressed on endothelium, the basement membrane, and pericytes, facilitating neutrophil extravasation [8]. During their transmigration across the endothelium and migration through the extracellular matrix (ECM) in the tissues, neutrophil proteases can facilitate cellular movement by cleaving proteins in the vascular endothelium and ECM [9-11]. Additionally, the activation of the fibrinolytic plasminogen (PLG)/tissue-type plasminogen activator (tPA)/urokinase-type plasminogen activator (uPA) system

contributes to neutrophil migration, adhesion, and thrombolysis [12-14]. In diseases characterized by excessive neutrophil-mediated inflammation, targeting neutrophil recruitment and activation may prevent further tissue damage and promote the resolution of inflammation [15,16].

Enolase-1 (ENO1, or alpha-enolase) is a glycolytic enzyme found in the cytosol, where it catalyzes the interconversion of 2-phosphoglycerate to phosphoenolpyruvate. It is ubiquitously expressed in most tissues. Interestingly, ENO1 has been detected on the surface of various cell types, including immune cells [17-20], cancer cells [21,22], and neuronal cells [23]. When expressed on the cell surface, ENO1 acts as a plasminogen receptor (PLGR), facilitating plasmin (PLA) activation and cell mobilization. ENO1-mediated PLG binding and PLA activation promote the migration and invasion of cancer [22,24] and immune cells [19], contributing to metastasis and inflammation, respectively. Additionally, ENO1 can serve as an autoantigen, eliciting anti-ENO1 autoantibodies in autoimmune and inflammatory diseases, including rheumatoid arthritis (RA) [25], systemic sclerosis (SSc) [26], systemic lupus erythematosus (SLE) [27], primary sclerosing cholangitis [28], inflammatory bowel disease [29], Behcet's disease [30], and primary membranous nephropathy [31]. ENO1 expression increases in the blood after acute injury and regulates subsequent inflammatory responses [32-34]. When released from injured cells, soluble ENO1 functions as a damage-associated molecular pattern (DAMP), activating monocytes [35], neutrophils, and endothelial cells [34]. Thus, ENO1 is a 'moonlighting protein' with diverse functions that depend on its cellular localization and the pathophysiological context.

The PLGR function of ENO1 has been detected on the surface of human monocytes [17], neutrophils [18], and B lymphocytes [20]. ENO1 expression on the surface of monocytic cells can be enhanced by lipopolysaccharide (LPS) stimulation. Furthermore, LPS challenge in mice promoted the recruitment of monocytic cells overexpressing ENO1, but not of cells expressing a truncated form of ENO1 lacking the PLG-binding site [19]. Although ENO1 is known to act as a PLGR on the cell surface, its role in regulating neutrophilic inflammation has not yet been investigated in vivo. Here, we demonstrate that neutrophils upregulate cell surface ENO1 expression in response to inflammatory stimulation. Additionally, neutrophil migration to sites of inflammation was attenuated by treatment with an anti-ENO1 monoclonal antibody (mAb). This antibody also neutralized the DAMP activity of ENO1. Our findings provide evidence that ENO1 plays a pivotal role in regulating neutrophil recruitment during acute inflammation.

Results

Surface ENO1 expression on neutrophils is upregulated following LPS stimulation both in vitro and in vivo

To investigate surface ENO1 expression on neutrophils during inflammation, we first isolated the neutrophils from mouse bone marrow and examined ENO1 expression using flow cytometry. Murine bone marrow neutrophils displayed basal surface ENO1 expression, which was significantly increased following LPS stimulation in vitro (Figure 1A). To assess whether surface ENO1 expression is also upregulated during in vivo inflammation, we analyzed ENO1 expression on neutrophils in mice challenged intraperitoneally (i.p.) with LPS. Neutrophils in the bone marrow and circulation exhibited higher surface ENO1 expression under systemic inflammation (Figure 1B). Similarly, in mice challenged intratracheally (i.t.) with LPS to induce acute lung injury (ALI), elevated surface ENO1 levels were observed on the neutrophils in the bone marrow and blood (Figure 1C). To explore the mechanism behind increased ENO1 expression on inflammatory neutrophils, we analyzed ENO1 at mRNA and protein levels. Neutrophils from LPS-challenged and control animals expressed similar levels of ENO1 mRNA (Figure 1D) and protein (Figure 1E), suggesting that the upregulation of surface ENO1 during acute inflammation may result from the exteriorization of cytosolic proteins.

Surface ENO1 on neutrophils is involved in pericellular proteolysis, which can be inhibited by an anti-ENO1 mAb

ENO1 has been identified as a PLGR that promotes PLM activation on the cell surface [17-19]. To confirm the interaction between ENO1 and PLG, we conducted a cell-free dot blot assay. As shown in Figure 2A, ENO1 and PLG interacted specifically with each

other, while no interaction was observed with the control protein, bovine serum albumin (BSA). We next assessed whether the anti-ENO1 mAb 7E5 could block the ENO1-PLG interaction using an ELISA-based protein binding assay. The 7E5 mAb significantly disrupted the ENO1-PLG interaction compared to the isotype control antibody (Figure 2B). To investigate whether increased ENO1 expression on the neutrophil surface during inflammation enhances PLM-mediated proteolysis, we performed a fibrinolytic assay using neutrophils isolated from mouse blood and bone marrow. Neutrophils from LPS-challenged mice showed elevated cell-surface PLM activity compared to neutrophils from naïve mice. This increase in proteolysis was abolished by the 7E5 mAb (Figure 2C). As a positive control, fibrinolytic activity was also blocked by tranexamic acid (TXA), a lysine analog that binds PLG and prevents its activation. These findings indicate that upregulated ENO1 expression on the neutrophil surface contributes to the enhancement of PLM-mediated proteolysis during inflammation.

ENO1 drives neutrophilic inflammation and tissue injury in the LPS-induced ALI mouse model

Since increased ENO1 expression enhances the pericellular proteolytic activity of neutrophils, we next investigated the role of ENO1 in neutrophil migration in vivo using the LPS-induced ALI mouse model, characterized by excessive neutrophil infiltration into the alveolar compartment [36]. Mice were intravenously (i.v.) administered 7E5 mAb or an isotype control antibody 2 hours before intratracheal (i.t.) instillation of LPS. At 24 hours post-challenge, mice were sacrificed, and bronchoalveolar lavage fluid (BALF) was analyzed for inflammatory cell infiltration and proinflammatory mediator production. Lung tissue sections were examined for histopathological changes. LPS-

challenged mice showed a robust influx of cells into the alveolar space, with the majority being neutrophils (Figure 3A). Administration of 7E5 mAb significantly reduced neutrophil infiltration (Figure 3B), the production of proinflammatory mediators (TNF, IL-6, and KC), and protein accumulation in BALF, an indicator of lung edema. Histopathological analysis further revealed that 7E5 mAb treatment decreased neutrophil accumulation in the alveolar and interstitial spaces and mitigated lung injury (Figure 3D).

We also examined the effect of ENO1 blockade on neutrophil extracellular trap (NET) formation, which is known to contribute to ALI [37]. Treatment with 7E5 mAb reduced the number of NETotic neutrophils containing citrullinated histone 3 (citH3) (Figures 4A and 4B) and lowered levels of soluble double-stranded DNA (dsDNA) in BALF (Figure 4C). Additionally, ENO1 blockade decreased the frequency of NETotic neutrophils in the blood (Figure 4B). These findings suggest that ENO1 plays a critical role in mediating neutrophilic inflammation and lung injury during LPS-induced ALI.

Anti-ENO1 mAb inhibits neutrophil recruitment in inflammation induced by cell injury

In the absence of infection, acute inflammation can be triggered by DAMPs released from injured cells, with recruited neutrophils potentially causing further tissue damage [38]. To investigate whether ENO1 plays a key role in regulating neutrophil migration during sterile inflammation, we injected necrotic EL4 cells intraperitoneally (i.p.) into mice pretreated with 7E5 mAb or control antibody. After 12 hours, we observed a robust influx of neutrophils and monocytes into the peritoneal cavity (Figure 5A). Treatment with 7E5 mAb significantly reduced the number of total peritoneal exudate

cells (PECs), as well as the recruitment of neutrophils and monocytes to the peritoneal cavity (Figure 5B). These results suggest that ENO1 plays an essential role in recruiting neutrophils to injured tissues during sterile inflammation.

7E5 mAb reduces inflammation induced by soluble ENO1

It has been reported that elevated levels of ENO1 can be detected in the plasma of post-trauma patients, and soluble ENO1 may directly stimulate the activation of innate immune cells [34,35]. In both LPS-induced ALI and necrotic cell-induced models of acute inflammation, serum ENO1 levels significantly increased following the inflammatory challenges (Figure 6A and 6B). We hypothesized that soluble ENO1 functions as a DAMP to stimulate tissue-resident macrophage activation, which could be blocked by 7E5 mAb. To test this hypothesis, we stimulated alveolar macrophage MH-S cells with recombinant ENO1 protein, in the presence or absence of 7E5 mAb. As shown in Figure 6C, ENO1 stimulation led to significant production of TNF and IL-6 by MH-S cells, and 7E5 mAb dose-dependently suppressed the inflammatory response. These results demonstrate that, in addition to blocking PLM-mediated neutrophil migration, the anti-ENO1 mAb 7E5 also attenuates inflammation by neutralizing the DAMP activity of ENO1.

Neutrophil migration can be pharmacologically attenuated by a PLG inhibitor

To confirm that PLG activation is required for neutrophil migration during inflammation, we investigated the effect of TXA, a clinically used PLG inhibitor, on neutrophil recruitment. Mice were i.v. administered PBS or TXA 0.5 hours before i.t. instillation of LPS. Twenty-four hours after the LPS challenge, the mice were sacrificed, and BALF was analyzed for inflammatory cell infiltration. Compared to the PBS-

treated group, the robust influx of neutrophils observed in LPS-challenged mice was significantly inhibited by TXA treatment (Figure 6A and 6B). Collectively, these results demonstrate that the PLG/PLM system plays a crucial role in mediating neutrophil migration during inflammation.

Discussion

Acute inflammation is essential for the host's immune defense against pathogens; however, excessive activation of immune effectors, such as neutrophils, can lead to collateral tissue damage and even organ failure in severe cases [6,7]. Therefore, it is crucial to identify molecules that contribute to the immune response and develop targeting agents to modulate inappropriate inflammation. In the present study, we found that surface ENO1 on neutrophils was upregulated during inflammation and promoted PLG activation, which may facilitate neutrophil migration through paracellular proteolysis. In LPS-induced ALI and necrotic cell-induced peritonitis mouse models, administration of anti-ENO1 mAb significantly attenuated neutrophilic inflammation. The anti-ENO1 mAb also neutralized the immunostimulatory activity of soluble ENO1, which was significantly increased in the circulation of animals after inflammatory challenges. These results suggest that ENO1 plays a key role in mediating neutrophilic inflammation and may serve as a target for treating diseases associated with excessive inflammation, such as ALI/ARDS.

ENO1 is known to be present on the surface of various immune cells, including neutrophils [17,18,20]. However, it remains unclear whether ENO1 expression on the neutrophil surface is altered during inflammation. Our data show that upon inflammatory stimulation, both in vitro and in vivo, neutrophils exhibit upregulated

surface ENO1 expression without changes in the overall levels of ENO1 mRNA and protein. This suggests that ENO1 is translocated to the surface from intracellular stores. Similar phenomena of ENO1 translocation have been observed in monocytes [19] and cancer cells [39,40]. In human breast cancer MDA-MB-231 cells, Ca^{2+} influx mediated by stromal interaction molecule (STIM) 1 and the calcium release-activated calcium (ORAI) 1 molecule regulates ENO1 exteriorization [39]. In human lung adenocarcinoma A549 cells, protein arginine methyltransferase 5 (PRMT5) was identified as responsible for ENO1 methylation and cell surface trafficking [40]. The molecular mechanism underlying ENO1 exteriorization in inflammatory neutrophils has not yet been identified, and whether similar mechanisms observed in cancer cells contribute to ENO1 translocation in neutrophils remains to be investigated.

The PLG/PLM system is crucial for fibrinolysis and promotes cell invasion by breaking down extracellular matrix proteins [19,22,41]. Our data show that inflammatory neutrophils exhibit enhanced fibrinolytic activity, which is blocked by the 7E5 mAb, specifically interrupting the interaction between ENO1 and PLG. In the LPS-induced ALI model, neutrophil recruitment was significantly inhibited by 7E5 mAb and the PLG inhibitor TXA, indicating that PLM-mediated proteolysis of the ECM is essential for the efficient migration of neutrophils to the inflammation site. Previous studies have presented differing perspectives on the role of PLG/PLM in neutrophil migration using PLM-deficient mice. Ploplis et al. reported that Plg (+/+) and Plg (-/-) mice showed similar neutrophil recruitment during thioglycolate-induced peritoneal inflammation [42]. However, in a biomaterial-induced peritonitis model, neutrophil recruitment was markedly reduced in Plg (-/-) mice [43]. Neutrophil infiltration in response to ischemia/reperfusion injury was also diminished in tPA (-/-) mice [12].

These discrepant observations may result from the use of different inflammation models in those studies. In our LPS-induced ALI and necrotic cell-induced peritonitis mouse models, our approach using pharmacological blockers of PLG/PLM activation supports the crucial role of PLM-mediated proteolysis in neutrophil transmigration during inflammation.

Our data showed that ENO1 was markedly elevated in the plasma following inflammation induced by LPS or necrotic cells. We also found that recombinant ENO1 was a potent activator of alveolar macrophages, suggesting that ENO1 released from injured cells may act as a DAMP to amplify the inflammatory response. In addition to catalyzing glycolysis in the cytosol, ENO1 is detected at various cellular locations, where it may stabilize the mitochondrial membrane, regulate gene expression, act as an RNA chaperone, or function as a PLGR [44]. ENO1 has also been shown to be released into the extracellular space as a soluble protein [35] or in exosomes [39,45]. Soluble ENO1 exhibits immunostimulatory activities [34,35], while ENO1-containing exosomes may enhance cancer cell migration and invasion [39]. In autoimmune diseases such as RA [35], SLE [27], and SSc [26], soluble ENO1 and anti-ENO1 autoantibodies can be detected in the circulation, with soluble ENO1 shown to activate the CD14-dependent TLR4 pathway in monocytes from both healthy individuals and RA patients [35]. In trauma-induced ALI and multiple organ failure, ENO1 levels were markedly increased in plasma, and ENO1 was shown to cause proinflammatory activation of pulmonary microvascular endothelial cells and prime neutrophils via plasmin activation of protease-activated receptor 2 [34]. In a rat model of spinal cord injury (SCI), levels of neuron-specific enolase (NSE) in serum and tissue were significantly increased after injury, and the administration of ENOblock, a small

molecule inhibitor of enolase, reduced serum levels of proinflammatory cytokines/chemokines, expression of matrix metalloproteinases (MMPs) in spinal cord tissues, and gliosis [32]. Besides functioning as a proinflammatory agonist, cell surface ENO1 may also bind other immunostimulatory molecules, such as apolipoprotein B, which promotes monocyte activation [46]. We found that blocking PLG activation using inhibitors such as TXA could attenuate PLM-facilitated neutrophil recruitment. However, targeting ENO1 using the 7E5 mAb may more effectively dampen inflammation, as it can block both the PLGR and immunostimulatory functions of ENO1.

In conclusion, our data demonstrate that during acute inflammation, the upregulated expression of ENO1 on the neutrophil surface and the release of soluble ENO1 from dying cells play key roles in mediating the neutrophilic inflammatory response. Targeting ENO1 using mAb appears to be an attractive strategy to attenuate inflammation, limit neutrophil recruitment, and reduce tissue damage. The anti-ENO1 7E5 mAb used in this study is a rat anti-mouse ENO1 mAb, generated as a surrogate for HL217, a humanized anti-human ENO1 mAb. Our data warrant further evaluation of HL217 in treating diseases associated with overt neutrophilic inflammation.

RESOURCE AVAILABILITY

Lead contact

Further information and requests for resources and reagents should be directed to and will be fulfilled by the lead contact, Chun-Jen Chen (cjchen1@ntu.edu.tw)

Materials availability

This study did not generate new unique reagents.

Data and code availability

- This paper does not report the original code.
- This paper does not report nucleotide sequencing-associated datasets, proteomics, peptidomics, metabolomics, structures of biological macromolecules, or small-molecule crystallography.
- Any additional information about the data reported in this paper is available from the lead contact upon request.

ACKNOWLEDGMENTS

This research was funded by National Taiwan University (109L104703-4, 111L893404, 112L892204, 113L890404). We thank HuniLife Biotechnology Inc. for providing proprietary anti-ENO1 mAbs 7E5 and HL217, and plasmid for recombinant protein expression. We thank NTU TechComm flow cytometry and qPCR core facilities.

AUTHOR CONTRIBUTIONS

Conceptualization: H.-Y.L., P.-H.H., N.-Y.C., Y.-J.Z. and C.-J.C.; methodology: H.-Y.L., P.-H.H., N.-Y.C., Y.-J.Z. and C.-J.C.; validation: H.-Y.L., P.-H.H., H.-W.C. and C.-J.C.; formal analysis: H.-Y.L., P.-H.H., and C.-J.C.; investigation: H.-Y.L., P.-H. H., T.-W.L., and H.-W.C.; resources: H.-Y.L., P.-H.H., T.-T.Y., and C.-J.C.; data curation: H.-Y.L and C.-J.C.; writing – original draft: H.-Y.L and C.-J.C.; writing – review and editing: H.-Y.L and C.-J.C.; visualization: H.-Y.L and C.-J.C.; supervision: C.-J.C.; project administration: C.-J.C.; funding acquisition: C.-J.C.

DECLARATION OF INTERESTS

The authors declare no competing interests.

REFERENCES

1. Burn, G.L., Foti, A., Marsman, G., Patel, D.F., and Zychlinsky, A. (2021). The Neutrophil. Immunity 54, 1377-1391. 10.1016/j.immuni.2021.06.006.
2. Tamassia, N., Bianchetto-Aguilera, F., Arruda-Silva, F., Gardiman, E., Gasperini, S., Calzetti, F., and Cassatella, M.A. (2018). Cytokine production by human neutrophils: Revisiting the "dark side of the moon". Eur J Clin Invest 48 Suppl 2, e12952. 10.1111/eci.12952.
3. Hawkins, C.L., and Davies, M.J. (2021). Role of myeloperoxidase and oxidant formation in the extracellular environment in inflammation-induced tissue damage. Free Radic Biol Med 172, 633-651. 10.1016/j.freeradbiomed.2021.07.007.
4. Castanheira, F.V.S., and Kubes, P. (2019). Neutrophils and NETs in modulating acute and chronic inflammation. Blood 133, 2178-2185. 10.1182/blood-2018-11-844530.
5. Soehnlein, O., Steffens, S., Hidalgo, A., and Weber, C. (2017). Neutrophils as protagonists and targets in chronic inflammation. Nat Rev Immunol 17, 248-261. 10.1038/nri.2017.10.
6. Wang, J., Li, Q., Yin, Y., Zhang, Y., Cao, Y., Lin, X., Huang, L., Hoffmann, D., Lu, M., and Qiu, Y. (2020). Excessive Neutrophils and Neutrophil Extracellular Traps in COVID-19. Front Immunol 11, 2063. 10.3389/fimmu.2020.02063.
7. Cesta, M.C., Zippoli, M., Marsiglia, C., Gavioli, E.M., Cremonesi, G., Khan, A., Mantelli, F., Allegretti, M., and Balk, R. (2023). Neutrophil activation and neutrophil extracellular traps (NETs) in COVID-19 ARDS and immunothrombosis. Eur J Immunol 53, e2250010. 10.1002/eji.202250010.

8. Schnoor, M., Vadillo, E., and Guerrero-Fonseca, I.M. (2021). The extravasation cascade revisited from a neutrophil perspective. Curr Opin Physiol 19, 119-128. 10.1016/j.cophys.2020.09.014.

9. Delclaux, C., Delacourt, C., D'Ortho, M.P., Boyer, V., Lafuma, C., and Harf, A. (1996). Role of gelatinase B and elastase in human polymorphonuclear neutrophil migration across basement membrane. Am J Respir Cell Mol Biol 14, 288-295. 10.1165/ajrcmb.14.3.8845180.

10. Hermant, B., Bibert, S., Concord, E., Dublet, B., Weidenhaupt, M., Vernet, T., and Gulino-Debrac, D. (2003). Identification of proteases involved in the proteolysis of vascular endothelium cadherin during neutrophil transmigration. J Biol Chem 278, 14002-14012. 10.1074/jbc.M300351200.

11. Zhu, Y., Huang, Y., Ji, Q., Fu, S., Gu, J., Tai, N., and Wang, X. (2021). Interplay between Extracellular Matrix and Neutrophils in Diseases. J Immunol Res 2021, 8243378. 10.1155/2021/8243378.

12. Uhl, B., Zuchtriegel, G., Puhr-Westerheide, D., Praetner, M., Rehberg, M., Fabritius, M., Hessenauer, M., Holzer, M., Khandoga, A., Furst, R., et al. (2014). Tissue plasminogen activator promotes postischemic neutrophil recruitment via its proteolytic and nonproteolytic properties. Arterioscler Thromb Vasc Biol 34, 1495-1504. 10.1161/ATVBAHA.114.303721.

13. Pluskota, E., Soloviev, D.A., Bdeir, K., Cines, D.B., and Plow, E.F. (2004). Integrin alphaMbeta2 orchestrates and accelerates plasminogen activation and fibrinolysis by neutrophils. J Biol Chem 279, 18063-18072. 10.1074/jbc.M310462200.

14. Pluskota, E., Soloviev, D.A., and Plow, E.F. (2003). Convergence of the adhesive and fibrinolytic systems: recognition of urokinase by integrin alpha Mbeta 2

as well as by the urokinase receptor regulates cell adhesion and migration. Blood 101, 1582-1590. 10.1182/blood-2002-06-1842.

15. Filep, J.G. (2022). Targeting Neutrophils for Promoting the Resolution of Inflammation. Front Immunol 13, 866747. 10.3389/fimmu.2022.866747.

16. Bartneck, M., and Wang, J. (2019). Therapeutic Targeting of Neutrophil Granulocytes in Inflammatory Liver Disease. Front Immunol 10, 2257. 10.3389/fimmu.2019.02257.

17. Miles, L.A., Dahlberg, C.M., Plescia, J., Felez, J., Kato, K., and Plow, E.F. (1991). Role of cell-surface lysines in plasminogen binding to cells: identification of alpha-enolase as a candidate plasminogen receptor. Biochemistry 30, 1682-1691. 10.1021/bi00220a034.

18. Redlitz, A., Fowler, B.J., Plow, E.F., and Miles, L.A. (1995). The role of an enolase-related molecule in plasminogen binding to cells. Eur J Biochem 227, 407-415. 10.1111/j.1432-1033.1995.tb20403.x.

19. Wygrecka, M., Marsh, L.M., Morty, R.E., Henneke, I., Guenther, A., Lohmeyer, J., Markart, P., and Preissner, K.T. (2009). Enolase-1 promotes plasminogen-mediated recruitment of monocytes to the acutely inflamed lung. Blood 113, 5588-5598. 10.1182/blood-2008-08-170837.

20. Lopez-Alemany, R., Longstaff, C., Hawley, S., Mirshahi, M., Fabregas, P., Jardi, M., Merton, E., Miles, L.A., and Felez, J. (2003). Inhibition of cell surface mediated plasminogen activation by a monoclonal antibody against alpha-Enolase. Am J Hematol 72, 234-242. 10.1002/ajh.10299.

21. Didiasova, M., Wujak, L., Wygrecka, M., and Zakrzewicz, D. (2014). From plasminogen to plasmin: role of plasminogen receptors in human cancer. Int J Mol Sci 15, 21229-21252. 10.3390/ijms151121229.

22. Hsiao, K.C., Shih, N.Y., Fang, H.L., Huang, T.S., Kuo, C.C., Chu, P.Y., Hung, Y.M., Chou, S.W., Yang, Y.Y., Chang, G.C., and Liu, K.J. (2013). Surface alpha-enolase promotes extracellular matrix degradation and tumor metastasis and represents a new therapeutic target. PLoS One 8, e69354. 10.1371/journal.pone.0069354.

23. Nakajima, K., Hamanoue, M., Takemoto, N., Hattori, T., Kato, K., and Kohsaka, S. (1994). Plasminogen binds specifically to alpha-enolase on rat neuronal plasma membrane. J Neurochem 63, 2048-2057. 10.1046/j.1471-4159.1994.63062048.x.

24. Principe, M., Ceruti, P., Shih, N.Y., Chattaragada, M.S., Rolla, S., Conti, L., Bestagno, M., Zentilin, L., Yang, S.H., Migliorini, P., et al. (2015). Targeting of surface alpha-enolase inhibits the invasiveness of pancreatic cancer cells. Oncotarget 6, 11098-11113. 10.18632/oncotarget.3572.

25. Kinloch, A., Tatzer, V., Wait, R., Peston, D., Lundberg, K., Donatien, P., Moyes, D., Taylor, P.C., and Venables, P.J. (2005). Identification of citrullinated alpha-enolase as a candidate autoantigen in rheumatoid arthritis. Arthritis Res Ther 7, R1421-1429. 10.1186/ar1845.

26. Terrier, B., Tamby, M.C., Camoin, L., Guilpain, P., Berezne, A., Tamas, N., Broussard, C., Hotellier, F., Humbert, M., Simonneau, G., et al. (2010). Antifibroblast antibodies from systemic sclerosis patients bind to alpha-enolase and are associated with interstitial lung disease. Ann Rheum Dis 69, 428-433. 10.1136/ard.2008.104299.

27. Li, M., Li, J., Wang, J., Li, Y., and Yang, P. (2018). Serum level of anti-alpha-enolase antibody in untreated systemic lupus erythematosus patients correlates with 24-hour urine protein and D-dimer. Lupus 27, 139-142. 10.1177/0961203317721752.

28. Orth, T., Kellner, R., Diekmann, O., Faust, J., Meyer zum Buschenfelde, K.H., and Mayet, W.J. (1998). Identification and characterization of autoantibodies against catalase and alpha-enolase in patients with primary sclerosing cholangitis. Clin Exp Immunol 112, 507-515. 10.1046/j.1365-2249.1998.00583.x.

29. Roozendaal, C., Zhao, M.H., Horst, G., Lockwood, C.M., Kleibeuker, J.H., Limburg, P.C., Nelis, G.F., and Kallenberg, C.G. (1998). Catalase and alpha-enolase: two novel granulocyte autoantigens in inflammatory bowel disease (IBD). Clin Exp Immunol 112, 10-16. 10.1046/j.1365-2249.1998.00528.x.

30. Lee, K.H., Chung, H.S., Kim, H.S., Oh, S.H., Ha, M.K., Baik, J.H., Lee, S., and Bang, D. (2003). Human alpha-enolase from endothelial cells as a target antigen of anti-endothelial cell antibody in Behcet's disease. Arthritis Rheum 48, 2025-2035. 10.1002/art.11074.

31. Wakui, H., Imai, H., Komatsuda, A., and Miura, A.B. (1999). Circulating antibodies against alpha-enolase in patients with primary membranous nephropathy (MN). Clin Exp Immunol 118, 445-450. 10.1046/j.1365-2249.1999.01080.x.

32. Haque, A., Capone, M., Matzelle, D., Cox, A., and Banik, N.L. (2017). Targeting Enolase in Reducing Secondary Damage in Acute Spinal Cord Injury in Rats. Neurochem Res 42, 2777-2787. 10.1007/s11064-017-2291-z.

33. Haque, A., Ray, S.K., Cox, A., and Banik, N.L. (2016). Neuron specific enolase: a promising therapeutic target in acute spinal cord injury. Metab Brain Dis 31, 487-495. 10.1007/s11011-016-9801-6.

34. Bock, A., Tucker, N., Kelher, M.R., Khan, S.Y., Gonzalez, E., Wohlauer, M., Hansen, K., Dzieciatkowska, M., Sauaia, A., Banerjee, A., et al. (2015). alpha-Enolase Causes Proinflammatory Activation of Pulmonary Microvascular Endothelial

Cells and Primes Neutrophils Through Plasmin Activation of Protease-Activated Receptor 2. Shock 44, 137-142. 10.1097/SHK.0000000000000394.

35. Guillou, C., Freret, M., Fondard, E., Derambure, C., Avenel, G., Golinski, M.L., Verdet, M., Boyer, O., Caillot, F., Musette, P., et al. (2016). Soluble alpha-enolase activates monocytes by CD14-dependent TLR4 signalling pathway and exhibits a dual function. Sci Rep 6, 23796. 10.1038/srep23796.

36. Aeffner, F., Bolon, B., and Davis, I.C. (2015). Mouse Models of Acute Respiratory Distress Syndrome: A Review of Analytical Approaches, Pathologic Features, and Common Measurements. Toxicol Pathol 43, 1074-1092. 10.1177/0192623315598399.

37. Liu, S., Su, X., Pan, P., Zhang, L., Hu, Y., Tan, H., Wu, D., Liu, B., Li, H., Li, H., et al. (2016). Neutrophil extracellular traps are indirectly triggered by lipopolysaccharide and contribute to acute lung injury. Sci Rep 6, 37252. 10.1038/srep37252.

38. Rock, K.L., Latz, E., Ontiveros, F., and Kono, H. (2010). The sterile inflammatory response. Annu Rev Immunol 28, 321-342. 10.1146/annurev-immunol-030409-101311.

39. Didiasova, M., Zakrzewicz, D., Magdolen, V., Nagaraj, C., Balint, Z., Rohde, M., Preissner, K.T., and Wygrecka, M. (2015). STIM1/ORAI1-mediated Ca2+ Influx Regulates Enolase-1 Exteriorization. J Biol Chem 290, 11983-11999. 10.1074/jbc.M114.598425.

40. Zakrzewicz, D., Didiasova, M., Kruger, M., Giaimo, B.D., Borggrefe, T., Mieth, M., Hocke, A.C., Zakrzewicz, A., Schaefer, L., Preissner, K.T., and Wygrecka, M. (2018). Protein arginine methyltransferase 5 mediates enolase-1 cell surface

trafficking in human lung adenocarcinoma cells. Biochim Biophys Acta Mol Basis Dis 1864, 1816-1827. 10.1016/j.bbadis.2018.02.021.

41. Deryugina, E.I., and Quigley, J.P. (2012). Cell surface remodeling by plasmin: a new function for an old enzyme. J Biomed Biotechnol 2012, 564259. 10.1155/2012/564259.

42. Ploplis, V.A., French, E.L., Carmeliet, P., Collen, D., and Plow, E.F. (1998). Plasminogen deficiency differentially affects recruitment of inflammatory cell populations in mice. Blood 91, 2005-2009.

43. Busuttil, S.J., Ploplis, V.A., Castellino, F.J., Tang, L., Eaton, J.W., and Plow, E.F. (2004). A central role for plasminogen in the inflammatory response to biomaterials. J Thromb Haemost 2, 1798-1805. 10.1111/j.1538-7836.2004.00916.x.

44. Didiasova, M., Schaefer, L., and Wygrecka, M. (2019). When Place Matters: Shuttling of Enolase-1 Across Cellular Compartments. Front Cell Dev Biol 7, 61. 10.3389/fcell.2019.00061.

45. Graner, M.W., Alzate, O., Dechkovskaia, A.M., Keene, J.D., Sampson, J.H., Mitchell, D.A., and Bigner, D.D. (2009). Proteomic and immunologic analyses of brain tumor exosomes. FASEB J 23, 1541-1557. 10.1096/fj.08-122184.

46. Lee, J.Y., Kang, M.J., Choi, J.Y., Park, J.S., Park, J.K., Lee, E.Y., Lee, E.B., Pap, T., Yi, E.C., and Song, Y.W. (2018). Apolipoprotein B binds to enolase-1 and aggravates inflammation in rheumatoid arthritis. Ann Rheum Dis 77, 1480-1489. 10.1136/annrheumdis-2018-213444.

47. Swamydas, M., Luo, Y., Dorf, M.E., and Lionakis, M.S. (2015). Isolation of Mouse Neutrophils. Curr Protoc Immunol 110, 3 20 21-23 20 15. 10.1002/0471142735.im0320s110.

48. Chen, C.J., Kono, H., Golenbock, D., Reed, G., Akira, S., and Rock, K.L. (2007). Identification of a key pathway required for the sterile inflammatory response triggered by dying cells. Nat Med 13, 851-856. 10.1038/nm1603.

Figure legends

Figure 1. ENO1 expression on neutrophil surface is upregulated in mice subjected to LPS-induced inflammation.

(A) Flow cytometry analysis of surface ENO1 expression on mouse bone marrow neutrophils treated ex vivo with LPS for 3 hours.

(B) Flow cytometry analysis of surface ENO1 expression on bone marrow (BM) and blood neutrophils from mice challenged i.p. with LPS for the specified time ($n = 3$).

(C) Flow cytometry analysis of surface ENO1 expression on bone marrow (BM) and blood neutrophils from mice 24 hours after i.t. challenge with PBS ($n = 2$) or LPS ($n = 4$).

(D) qRT-PCR analysis of ENO1 mRNA expression in neutrophils from mice challenged i.p. with LPS for the specified time.

(E) Western blot analysis of ENO1 protein expression. Changes in ENO1 signals (normalized to actin signals) are expressed as fold changes relative to the 0-h group and indicated below each lane.

Data are representative of two (A and B) or three (C and E) independent experiments. Data in (D) are combined from four independent experiments. Data are presented as mean ± SEM. $*p < 0.05$, $**p < 0.01$, $***p < 0.001$.

Figure 2. The anti-ENO1 mAb 7E5 interrupts ENO1-PLG interaction and inhibits the fibrinolytic activity of inflammatory neutrophils.

(A) Dot blotting analysis showing specific interaction between ENO1 and PLG.

(B) ELISA-based protein binding assay showing the binding of PLG to plate-bound ENO1 in the presence of 7E5 or isotype control antibodies.

516 (C) Fibrinolytic activity analysis of neutrophils from mice 12 hours after i.p. challenge
517 with PBS or LPS, performed in the presence of 7E5 mAb, isotype control antibody, or
518 TXA ($n = 3$).
519 Data in (A) and (C) are representative of two independent experiments. Data in (B) are
520 combined from four independent experiments performed in duplicates. Data are
521 presented as mean ± SEM. *$p < 0.05$, **$p < 0.01$, ***$p < 0.001$.
522
523 **Figure 3. ENO1 blockade reduces the recruitment of neutrophils and attenuates**
524 **LPS-induced lung injury and inflammation.**
525 (A) Representative flow cytometry density plots and gating strategies of BALF cells
526 from mice 24 hours after i.t. challenge with LPS. The $Ly6G^{+}Ly6B.2^{+}$ gate represents
527 neutrophils.
528 (B) Total cell counts, and neutrophil percentages and counts in BALF of LPS-
529 challenged mice treated with 7E5 or isotype control antibodies. Mice challenged i.t.
530 with PBS served as the negative control.
531 (C) Cytokine and protein levels in BALF.
532 (D) Representative images of H&E-stained sections of mouse lungs and quantitative
533 scoring of lung injury.
534 Data in (B) and (C) are combined from three independent experiments. Data in (D) are
535 combined from two independent experiments. Data are presented as mean ± SEM. *p
536 < 0.05, **$p < 0.01$, ***$p < 0.005$, ****$p < 0.001$.
537
538 **Figure 4. ENO1 blockade reduces NETotic neutrophils in LPS-induced ALI.**

539 (A) Representative flow cytometry density plots and gating strategies of
540 $Ly6G^{+}citH3^{+}$ NETotic neutrophils in BALF and blood 24 hours after i.t. challenge with
541 PBS, LPS + isotype antibody, or LPS + 7E5 mAb.
542 (B) Frequencies and numbers and NETotic neutrophils in BALF and blood.
543 (C) Cell-free dsDNA levels in BALF.
544 Data in (B) and (C) are combined from three independent experiments and presented
545 as mean ± SEM. $**p < 0.01$, $***p < 0.005$.
546
547 **Figure 5. Anti-ENO1 mAb blocked neutrophil recruitment in inflammation**
548 **triggered by cell injury.**
549 (A) Representative flow cytometry density plots and gating strategies of PECs from
550 mice 12 hours after i.p. challenge with necrotic EL4 cells. The $CD11b^{+}Ly6C^{+}Ly6G^{-}$ and
551 $CD11b^{+}Ly6C^{+}Ly6G^{+}$ gates represent monocytes and neutrophils, respectively.
552 (B) Frequencies and counts of total PECs, monocytes, and neutrophils recruited to the
553 peritoneal cavity.
554 Data are combined from two independent experiments and are presented as mean ±
555 SEM. $**p < 0.01$, $***p < 0.005$.
556
557 **Figure 6. 7E5 mAb reduces inflammation stimulated by soluble ENO1.**
558 (A) ELISA analysis of soluble ENO1 in plasma from mice 24 hours after i.t. challenge
559 with PBS or LPS.
560 (B) ELISA analysis of soluble ENO1 in plasma from mice 12 hours after i.p. challenge
561 with PBS of necrotic EL4 cells.

562 (C) ELISA analysis of TNF and IL-6 produced by MH-S cells 20 hours after rENO1
563 stimulation in the absence or presence of 7E5 mAb or isotype control antibodies at the
564 specified dose.
565 Data in (A) and (B) are combined from two and three independent experiments,
566 respectively. Data in (C) are representative of three independent experiments. Data are
567 presented as mean ± SEM. $^{**}p < 0.01$, $^{***}p < 0.005$, $^{****}p < 0.001$.
568
569 **Figure 7. Neutrophil migration can be attenuated pharmacologically by a PLG**
570 **inhibitor.**
571 (A) Representative flow cytometry density plots and gating strategies of BALF cells
572 from mice 24 hours after i.t. challenge with LPS. The $CD11b^{+}$ $Ly6C^{+}Ly6G^{+}$ gate
573 represents neutrophils.
574 (B) Total cell counts, and neutrophil percentages and counts in BALF of LPS-
575 challenged mice treated with PBS or TXA. Mice challenged i.t. with PBS served as
576 negative controls.
577 Data are combined from two independent experiments and presented as mean ± SEM.
578 $^{***}p < 0.005$.

STAR METHODS

KEY RESOURCES TABLE

REAGENT or RESOURCE	SOURCE	IDENTIFIER
Antibodies		
Rabbit recombinant monoclonal ENO1 antibody	Abcam	Cat# ab227978; RRID:AB_2827927
Mouse monoclonal beta Actin antibody	Santa Cruz Biotechnology	Cat# sc-47778; RRID:AB_626632
Goat Polyclonal Plasminogen antibody, Biotin	Abcam	Cat# ab7335, RRID:AB_305860)
Donkey Anti-Rabbit IgG, Whole Ab ECL Antibody, HRP Conjugated	GE	Cat# NA934, RRID:AB_772206)
Anti-mouse/human CD11b Antibody, PE/Cyanine7	BioLegend	Cat# 101215, RRID:AB_312798
Anti-mouse Ly-6G Antibody, FITC	BioLegend	Cat# 127606, RRID:AB_1236494
Anti-mouse Ly-6C Antibody, Biotin	BioLegend	Cat# 128004, RRID:AB_1236553
Rat anti mouse Ly-6B.2, Biotin	Bio-Rad	Cat# MCA771B, RRID:AB_323346
Anti-mouse Ly-6G Antibody, Biotin	BioLegend	Cat# 127604, RRID:AB_1186108
PE Goat anti-rat IgG (minimal x-reactivity) Antibody	BioLegend	Cat# 405406, RRID:AB_315017
PE Donkey anti-rabbit IgG (minimal x-reactivity) Antibody	BioLegend	Cat# 406421, RRID:AB_2563484
Anti-Histone H3 (citrulline R2 + R8 + R17) antibody	Abcam	Cat# ab5103, RRID:AB_304752
Mouse anti-Rat IgG (H+L) Secondary Antibody, Biotin	Thermo Fisher Scientific	Cat# 13-4813-85, RRID:AB_466659
Proprietary rat anti-ENO1 antibody (7E5)	HuniLife Biotechnology, Inc.	N/A
Proprietary anti-ENO1 antibody (HL217)	HuniLife Biotechnology, Inc.	N/A
Rat IgG-UNLB (Rat IgG Isotype control)	SouthernBiotech	Cat# 0108-01, RRID:AB_2793932
FITC Annexin V	BioLegend	Cat# 640906
Bacterial and virus strains		
BL21(DE3)	N/A	N/A
Biological samples		
Mouse Blood	This paper	N/A
Mouse lung	This paper	N/A
Mouse bone marrow	This paper	N/A
Chemicals, peptides, and recombinant proteins		
RPMI-1640	Cytiva (Hyclone)	Cat# H30027.02
Fetal bovine serum (FBS)	Peak Serum	Cat# PS-FB2
Penicillin-Streptomycin-Amphotericin B	Biological Industries	Cat# 03-033-1B

Beta-mercaptoethanol	Cyrusbioscience Inc.	Cat# 101-60-24-2
Dulbecco's phosphate-buffered saline (DPBS)	Corning	Cat# 21-031-CM
Percoll	GE	Cat# 17-0891-01
Fc blocking buffer (2.4G2 mAb)	N/A	N/A
APC-conjugated streptavidin	BioLegend	Cat# 405207
7-AAD Viability Staining Solution	BioLegend	Cat# 420404
MojoSort™ Streptavidin Nanobeads	BioLegend	Cat# 480016
Qiazol	Qiagen	Cat# 79306
iQ SYBR Green supermix	Bio-Rad	Cat# 1708882
protease-inhibitor cocktail	Sigma-Aldrich	Cat# P8340
Tween 20	Cyrusbioscience Inc.	Cat# 101-9005-64-5
BSA	BioVision	Cat# 7906
Recombinant ENO1	N/A	N/A
Plasminogen	Sigma-Aldrich	Cat# 528180
10X blocking buffer	Abcam	Cat# ab126587
Peroxidase-conjugated avidin	BioLegend	Cat# 405103
ELISA diluent	eBioscience	Cat# 00-4202-56
TMB substrate solution	BioLegend	Cat# 421101
Lipopolysaccharide	Sigma-Aldrich	Cat# SI-L2630
Tranexamic acid	Daiichi Sankyo Taiwan Ltd.	N/A
Glu-plasminogen	Technoclone	Cat# I-TC41005
Urokinase	Green Cross Co., Ltd.	N/A
Chromogenix S-2251™	diapharma	Cat# S820332
isopropyl β-D-1-thiogalactopyranoside	Sigma-Aldrich	Cat# #367-93-1
Detoxi-Gel™ Endotoxin Removing Gel	Thermo Scientific	Cat# 20339
HisTrap FF Crude histidine-tagged protein purification columns	GE	Cat# 29048631
Critical commercial assays		
Deoxy+ HiSpec Reverse Transciptase kit	Yeastern Biotech Inc.	Cat# XR-LYT501
ELISA MAX™ Deluxe Set Mouse TNF-α	BioLegend	Cat# 430916
ELISA MAX™ Deluxe Set Mouse IL-6	BioLegend	Cat# 431301
Mouse KC/CXCL1 ELISA Development Kit	Peprotech	Cat# 900-K127
Pierce™ BCA Protein Assay Kits	Thermo Scientific	Cat# 23225
Qubit™ dsDNA BR Assay Kit	Invitrogen	Cat# Q32853
ToxinSensor™ Single Test Kit	GenScript	Cat# L00856-20
Experimental models: Cell lines		
EL4	N/A	N/A
MH-S	N/A	N/A
Experimental models: Organisms/strains		
Mouse: C57BL/6JNarl	NARLabs (Taipei, Taiwan)	N/A
Oligonucleotides		
Primers for mouse ENO1 Forward: AGCGATCCTACTGCCAGAAAT Reverse: GATCGACCTCAACAGTGGGA	Genomics BioSci & Tech. Co.Ltd.	N/A

Primers for mouse ACTB Forward:AGGTATCCTGACCCTGAAG Reverse:GCTCATTGTAGAAGGTGTGG	Genomics BioSci & Tech. Co.Ltd.	N/A
Recombinant DNA		
pTrcHis-ENO1 expressing vector	HuniLife Biotechnology, Inc.	N/A
Software and algorithms		
GraphPad Prism 8	Graphpad	https://www.graphpad.com
FlowJo_V10	BD Biosciences	https://www.flowjo.com
Image J	Image J	https://imagej.net/ij/

EXPERIMENTAL MODEL AND STUDY PARTICIPANT DETAILS

Cell lines

Murine T lymphoblast EL4 cells and murine alveolar macrophage MH-S cells were cultured in RPMI-1640 medium (Cytiva, MA) supplemented with 10% fetal bovine serum (FBS, Peak Serum, FL), penicillin/streptomycin/amphotericin B (Biological Industries, Israel), and 0.05 mM beta-mercaptoethanol (Cyrusbioscience Inc., Taipei, Taiwan). All cells were maintained at 37°C in a humidified atmosphere with 5% CO_2. Proprietary ENO1 monoclonal antibodies 7E5 and HL217 (patent: US9382331B2) were provided by HuniLife Biotechnology Inc.

Mice

Male C57BL/6 mice were purchased from the National Laboratory Animal Center (Taipei, Taiwan). The mice were housed under standard 12-hour light/dark cycle conditions in rooms with controlled temperature (22 ± 2°C) and humidity (50 ± 10%). All animal studies were approved by the Institutional Animal Care and Use Committee of National Taiwan University (Approval number: NTU-113-EL-00011).

METHOD DETAILS

600 **Isolation of mouse neutrophils from bone marrow and peripheral blood**

601 Mouse bone marrow neutrophils were isolated from the femurs and tibias of mice (6-
602 12 weeks old) using a modified procedure as described previously [47]. Briefly, bone
603 marrow cells were flushed from the bones using Dulbecco's phosphate-buffered saline
604 (DPBS, Corning, NY) containing 2% FBS and 5 mM EDTA. Neutrophils were purified
605 by centrifugation using 62.5% of Percoll (30 minutes at 1000 x g). After centrifugation,
606 the cells beneath the 62.5% Percoll layer were collected and washed with DPBS twice,
607 and treated with Ammonium-Chloride-Potassium (ACK) lysis buffer to remove
608 erythrocytes. In some experiments, mouse bone marrow neutrophils and peripheral
609 blood neutrophils were isolated by $Ly6G^{+}$ positive selection (BioLegend, CA) and
610 pooled together.

611

612 **Flow Cytometry**

613 To analyze cell surface markers, single-cell suspensions were first incubated with Fc
614 blocking buffer (2.4G2 mAb) for 15 minutes at 4°C, followed by incubation with
615 PE/Cyanine7-conjugated anti-mouse/human CD11b (BioLegend), FITC-conjugated
616 anti-mouse Ly6G (BioLegend), Biotin-conjugated anti-mouse Ly6B.2 (Bio-Rad, CA),
617 Biotin-conjugated anti-Ly6C (BioLegend) for 30 minutes at 4°C. After washing, the
618 cells were then incubated with APC-conjugated streptavidin (BioLegend) for 30
619 minutes at 4°C. Dead cells were excluded using 7-AAD staining. For surface ENO1
620 expression staining, single-cell suspensions were first incubated with mouse serum for
621 15 minutes at 4°C, followed by incubation with rat-anti mouse ENO1 mAb (7E5 mAb;
622 provided from HuniLife Biotechnology Inc., Taiwan) and PE-conjugated goat anti-rat
623 IgG (BioLegend) 30 minutes at 4°C. Afterward, the cells were stained with the cell
624 surface markers. For NETosis staining, single-cell suspensions were incubated with Fc

625 blocking buffer for 15 minutes at 4°C, followed by incubation with anti-citrullinated
626 histone 3 (citH3) antibody (Abcam, UK), PE/Cyanine7-conjugated anti-mouse/human
627 CD11b (BioLegend) and FITC-conjugated anti-mouse Ly6G (BioLegend) for 60
628 minutes at 4°C, The cells were then incubated with PE-conjugated donkey anti-rabbit
629 IgG (BioLegend) for 30 minutes at 4°C. Samples were analyzed on a FACSCanto II
630 flow cytometer (BD Biosciences, NJ), and data, including median fluorescence
631 intensity (MFI), were analyzed using FlowJo software (BD Biosciences).
632
633 **RNA extraction and real-time quantitative PCR (RT-qPCR)**
634 Total RNA was purified from cell samples using Qiazol (Qiagen, Germany). Reverse
635 transcription was performed using the Deoxy+ HiSpec Reverse Transcriptase kit
636 (Yeastern Biotech Inc., Taiwan). Quantitative real-time PCR was carried out using the
637 iQ SYBR Green supermix (Bio-Rad) according to the manufacturer's protocol on a
638 CFX Connect thermal cycler (Bio-Rad). mRNA expression was normalized to *ACTB*
639 (β-actin) and calculated using the 2^(–ΔΔCT) method. The primers used in this study
640 were as follows: For *ENO1*, forward 5'-AGCGATCCTACTGCCAGAAAT-3' and
641 reverse 5'-GATCGACCTCAACAGTGGGA-3'; for *ACTB*, forward 5'-
642 AGGTGTGCACCTTTTATTGGTCTCAA-3' and reverse 5'-
643 TGTATGAAGGTTTGGTCTCCCT-3'.
644
645 **Western blotting**
646 The purified neutrophils ($Ly6^+$ cells) were lysed in radioimmunoprecipitation assay
647 (RIPA) buffer containing a protease inhibitor cocktail (Sigma-Aldrich, MO) and
648 denatured at 95°C for 10 minutes. Samples were run on 10% SDS-PAGE gels and
649 transferred onto a PVDF membrane (Millipore, MA). Immunoblots were blocked in

650 TBS (tris-buffered saline) containing 0.1% Tween 20 (Cyrusbioscience Inc.) and 2%
651 bovine serum albumin (BSA, BioVision, CA) for 1 hour at room temperature, then
652 probed with primary antibodies for ENO1 (Abcam) and β-actin (Santa Cruz, CA)
653 overnight at 4°C. After extensive washes by TBS containing 0.1% Tween-20 (TBST),
654 immunoblots were incubated with horseradish peroxidase-conjugated secondary
655 antibodies (GE, Il), and signals were detected using chemiluminescence.
656
657 **Dot blotting analysis**
658 To detect the interaction between ENO1 and PLG, 1 μg of each protein was blotted on
659 the strip of PVDF membrane and 1 μg of BSA was blotted as a negative control. After
660 blocking with 2% BSA/TBST for 1 hour at room temperature, the membranes were
661 incubated with 1 μg/ml of ENO1 or PLG in phosphate-buffered saline (PBS) for 1 hour
662 at room temperature. The membranes were then probed with primary antibodies for
663 ENO1 (Abcam) and plasminogen (Abcam) for 1 hour at room temperature. After
664 extensive washes by TBST, immunoblots were incubated with horseradish peroxidase-
665 conjugated secondary antibodies (GE, IL) or peroxidase-conjugated avidin
666 (BioLegend), and signals were detected using chemiluminescence.
667
668 **ELISA-based protein binding assay**
669 To assess the inhibitory effect of 7E5 mAb on ENO1-PLG interaction, 10 μg/ml of
670 ENO1 was coated on the 96-well microplate (Corning) overnight at 4°C. After blocking
671 with ELISA diluent (eBioscience, CA) for 1 hour at room temperature, the wells were
672 incubated with ELISA diluent containing with indicated concentration of 7E5 mAb or
673 isotype control (SouthernBiotech, AL) for 2 hours at room temperature. The wells were
674 then incubated with ELISA diluent containing 10 μg/ml of plasminogen for 2 hours at

675 room temperature. Afterward, the wells were hybridized with an antibody against
676 plasminogen (Abcam) for 1 hour at room temperature, followed by incubation with
677 avidin-HRP (BioLegend) for 30 minutes at room temperature. The signals from the
678 microplate plate were visualized using the TMB substrate solution (BioLegend) and
679 read at 650 nm
680
681 **LPS-induced acute lung injury (ALI) mouse model**
682 8 to 12 weeks-old male wild-type (WT) C57BL/6 mice received a single intratracheal
683 instillation of lipopolysaccharide (LPS, Sigma-Aldrich) at 2 mg/kg (dissolved in 50 μL
684 of DPBS) or DPBS only (sham). In some experiments, anti-ENO1 mAb at 5 mg/kg and
685 tranexamic acid at 100 mg/kg were administered intravenously for 2 hours and 1 hour,
686 respectively, before the induction of lung injury. Mice were sacrificed at 6, 12, or 24
687 hours after induction of lung injury.
688
689 **Bronchoalveolar Lavage and BALF analysis**
690 Bronchoalveolar lavage (BAL) was performed using the modified procedure as
691 described previously [36]. Briefly, 0.5 mL of PBS containing 5 mM EDTA was instilled
692 into the trachea four times via a 24G I.V. catheter (Terumo, Japan), and bronchial
693 alveolar lavage fluids (BALF) were collected. After centrifugation (350 x g, 5 minutes),
694 the supernatant of BALF was collected and stored at -20°C for further experiments. The
695 BALF cells were resuspended, counted using a hemocytometer, and analyzed by flow
696 cytometry as described previously. Measurement of cytokines and chemokines was
697 performed using ELISA kits for mouse TNF-α (BioLegend), mouse IL-6 (BioLegend),
698 and mouse KC (Peprotech, NJ) according to the manufacturer's instructions. Total
699 protein and dsDNA in the BALF were measured using the Pierce™ BCA Protein Assay

700 Kits (Thermo Scientific, MA) and Qubit™ dsDNA BR Assay Kit (Invitrogen, CA)
701 following the manufacturer's instructions.
702
703 **Measurement of soluble ENO1 by ELISA**
704 96-well plates were coated with anti-ENO1 monoclonal antibody, HL217, in PBS
705 overnight at 4°C. After blocking with blocking buffer (Abcam) for 1 hour at room
706 temperature, the wells were incubated with blocking buffer containing the indicated
707 concentration of rENO1 as standard and mouse serum or plasma sample for 2 hours at
708 room temperature. The wells were then incubated with a blocking buffer containing 1
709 μg/ml of 7E5 mAb for 1 hour at room temperature. Afterward, the wells were
710 hybridized with biotinylated antibodies against Rat IgG (eBioscience) for 1 hour at
711 room temperature, followed by avidin-HRP (BioLegend) for 30 minutes at room
712 temperature. The signals from the microplate were visualized using TMB substrate
713 solution (BioLegend) and measured at 650 nm.
714
715 **Cell surface-associated fibrinolytic assay**
716 The purified neutrophils ($Ly6^+$ cells) were washed and resuspended in DPBS at a
717 concentration of 2 x 10^6/mL. They were preincubated with the indicated concentration
718 of 7E5 mAb, isotype control antibody, or tranexamic acid (TXA, Daiichi Sankyo
719 Taiwan Ltd., Taiwan) for 30 minutes, then incubated with 500 nM Glu-plasminogen
720 (Technoclone, Austria) for 1 hour. After incubation, the cells were washed with DPBS
721 three times to remove unbound PLG and resuspended in DPBS. Then, 10U of urokinase
722 (Taiwan Green Cross Co., Ltd., Taiwan) and 0.2 mM plasminogen chromogenic
723 substrate Chromogenix S-2251™ (Diapharma, OH) were added to the cell suspension

724 and incubated at 37°C for 3 hours. The cell surface plasmin activity was measured by
725 absorbance at 405 nm.
726
727 **Preparation of necrotic cell**
728 Cell necrosis was induced by the heat-shocked method as previously described [48].
729 Briefly, EL4 cells were harvested by centrifugation (350 x g, 5 minutes), washed twice
730 with 10ml of DPBS, and resuspended in DPBS at a density of 4×10^7 cells/mL. The
731 EL4 cells were heat-shocked at 45°C for 10 minutes, followed by incubation at 37°C
732 for 5 hours to induce necrosis. The necrotic EL4 cells were confirmed by flow
733 cytometry (annexin V^+, 7-AAD^+).
734
735 **Necrotic cell-induced peritonitis mouse model**
736 Male C57BL/6 mice, 8 to 12 weeks old, were injected i.p. with 2 $x10^7$ necrotic EL4
737 cells (in 0.5 ml of PBS) to induce sterile peritonitis. Mice in the sham control group
738 received 0.5 mL of PBS only. The 7E5 mAb (5 mg/kg) was administered i.p. 2 hours
739 before the induction of sterile peritonitis. Twelve hours after the challenge, the mice
740 were sacrificed. Serum or plasma samples were collected, and peritoneal exudate cells
741 (PECs) were harvested by peritoneal lavage using 7 mL of harvest solution (PBS
742 containing 2% FBS and 5 mM EDTA). PECs were counted using a hemocytometer and
743 analyzed by flow cytometry.
744
745 **Histopathology**
746 Mouse lung tissues were perfused and fixed in 10% formalin. The tissue sections were
747 embedded in paraffin and stained with H&E (performed by Histology Center, Institute
748 of Molecular and Comparative Pathobiology, National Taiwan University). The degree

749 of lung injury was graded by the veterinarian and using the scoring system described in
750 a previous study [36]. Briefly, the lung section were scored 0-2 by the parameters of
751 neutrophils in the alveolar space, neutrophils in the interstitial space, proteinaceous
752 debris filling the airspaces, and alveolar septal thickening. For each sample, twenty
753 high-magnification fields were randomly counted, and the total score would be
754 calculated by the following formula: $[(20 \times A) + (14 \times B) + (7 \times C) + (2 \times D)]/20 \times 72)$.
755

756 **Expression of recombinant ENO1**

757 "The enolase-1 protein gene was cloned into the pTrcHis vector and expressed in
758 BL21(DE3) cells. A single colony was picked and inoculated in lysogeny broth (LB
759 broth) containing 100 μg/ml of ampicillin and incubated overnight at 37°C, 140 rpm.
760 The overnight culture was transferred to fresh LB broth containing 100 μg/ml of
761 ampicillin and incubated at 37°C, 140 rpm for 1-2 hours. When the optical density
762 (OD600) reached 0.6, isopropyl β-D-1-thiogalactopyranoside (IPTG, Sigma) was
763 added to a final concentration of 0.7 mM for overnight induction at 25°C, 140 rpm for
764 16 hours. The cells were collected by centrifugation at 10,000 x g for 10 minutes. The
765 supernatants were discarded, and the cell pellets were resuspended in an appropriate
766 volume (wet cell pellets weight: buffer volume = 1:5) of binding buffer (20 mM
767 NaH_2PO_4, 0.5 M NaCl, 5 mM imidazole, pH 7) containing protease inhibitor cocktail
768 (Sigma-Aldrich), and lysed using Constant System (25 kpsi). The supernatants were
769 collected, and the ENO1 protein was purified using HisTrap FF Crude histidine-tagged
770 protein purification columns (GE) according to the manufacturer's instructions. The
771 purity of ENO1 was assessed by SDS-PAGE and western blotting. The purified protein
772 was then desalted using HiTrap Desalting columns (GE) and endotoxin were removed
773 using Detoxi-Gel™ Endotoxin Removing Gel (Thermo Scientific) according to the

774 manufacturer's instructions. The endotoxin level was determined to be < 0.03 EU/ml
775 using the ToxinSensor™ Single Test Kit (GenScript, NJ).
776
777 **Statistics**
778 Statistical analyses were performed using GraphPad Prism 8, and data are expressed as
779 the mean ± standard error of the mean (SEM). Comparisons between two groups were
780 conducted using an unpaired Student's *t*-test. For comparisons among multiple groups,
781 a one-way ANOVA with Tukey's post hoc test was used. Statistical significance was
782 defined as $p < 0.05$.

Figure 1. ENO1 expression on neutrophil surface is upregulated in mice subjected to LPS-induced inflammation

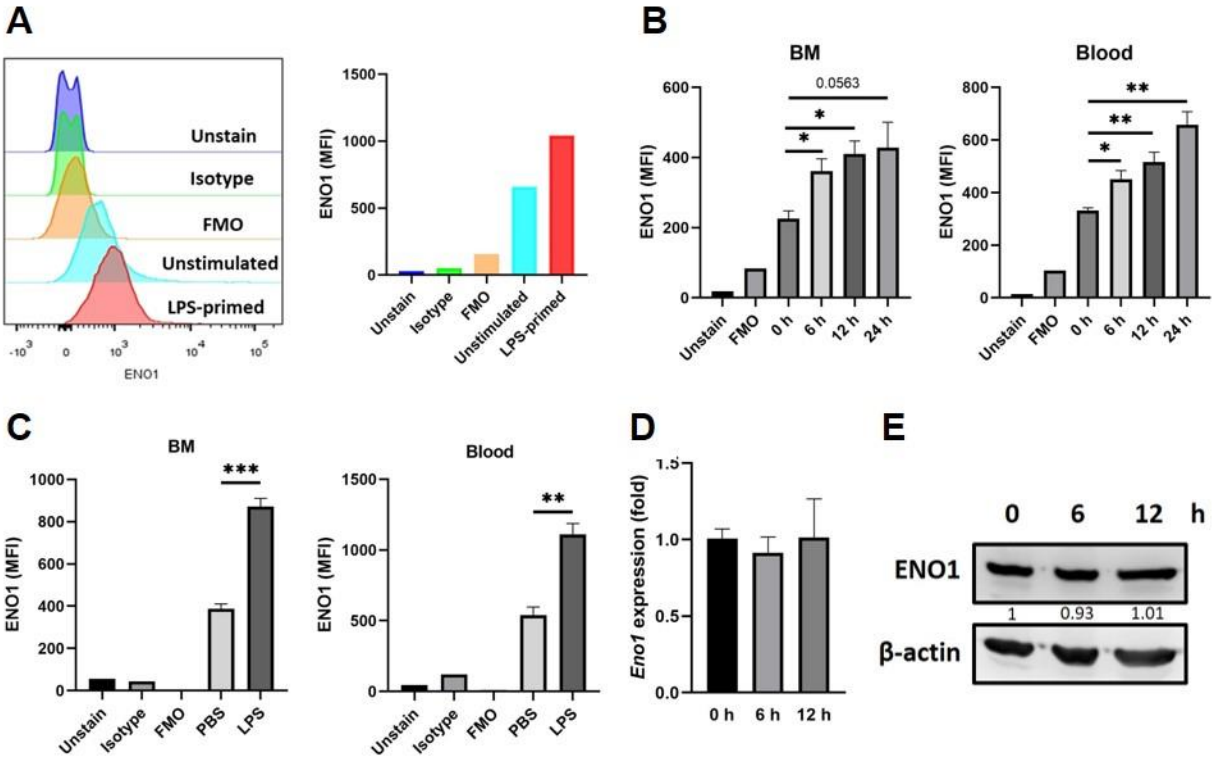

Figure 2. The anti-ENO1 mAb 7E5 interrupts ENO1-PLG interaction and inhibits the fibrinolytic activity of inflammatory neutrophils

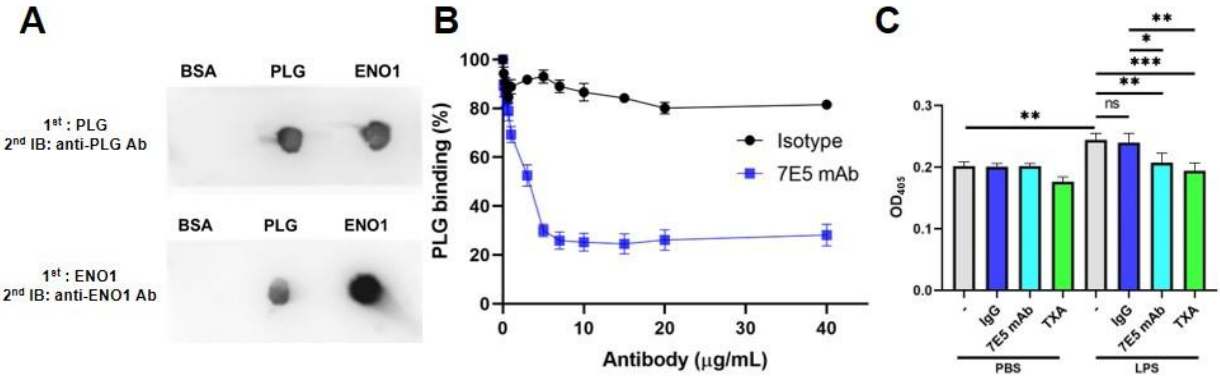

Figure 3. ENO1 blockade reduces the recruitment of neutrophils and attenuates LPS-induced lung injury and inflammation

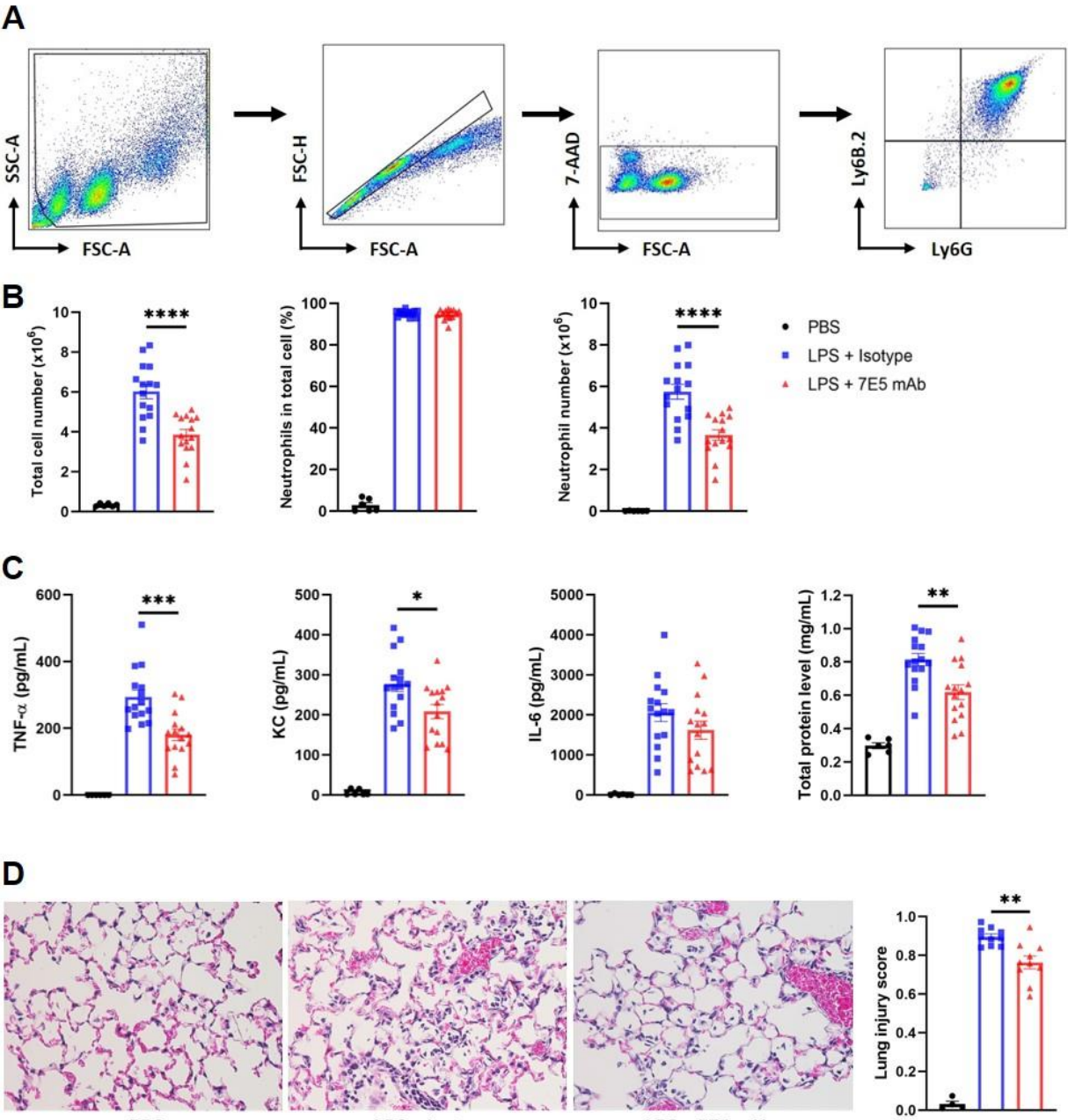

Figure 4. ENO1 blockade reduces NETotic neutrophils in LPS-induced ALI.

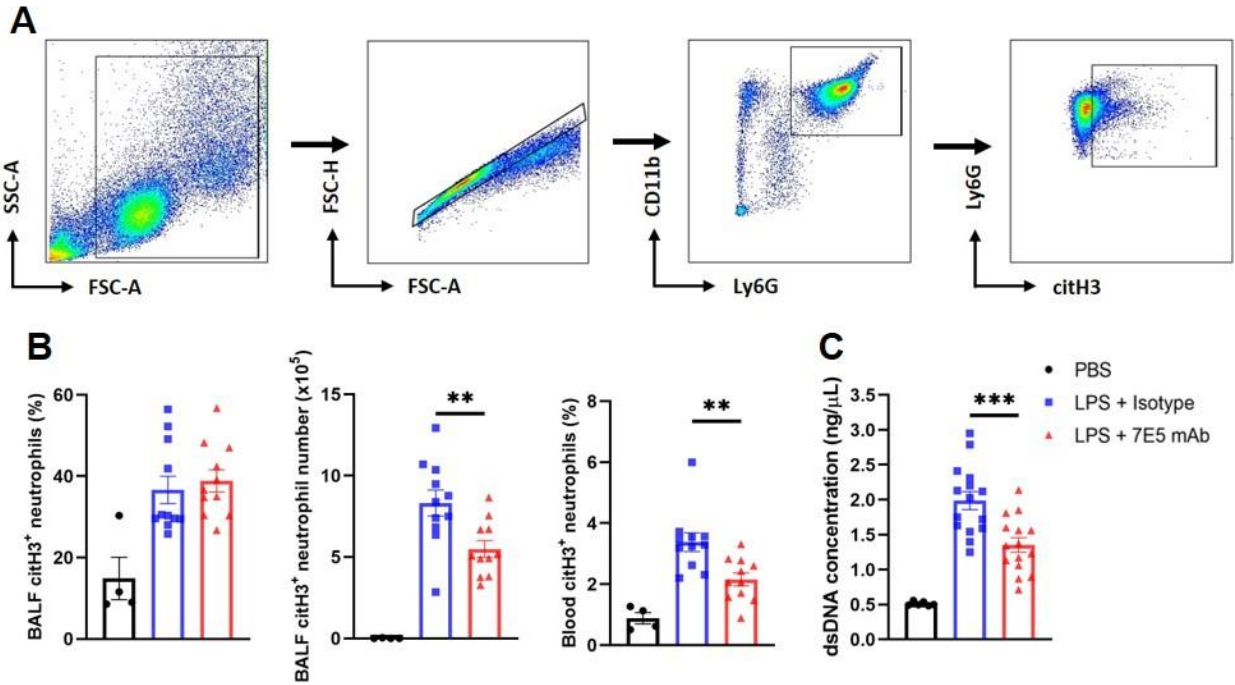

Figure 5. Anti-ENO1 mAb blocked neutrophil recruitment in inflammation triggered by cell injury

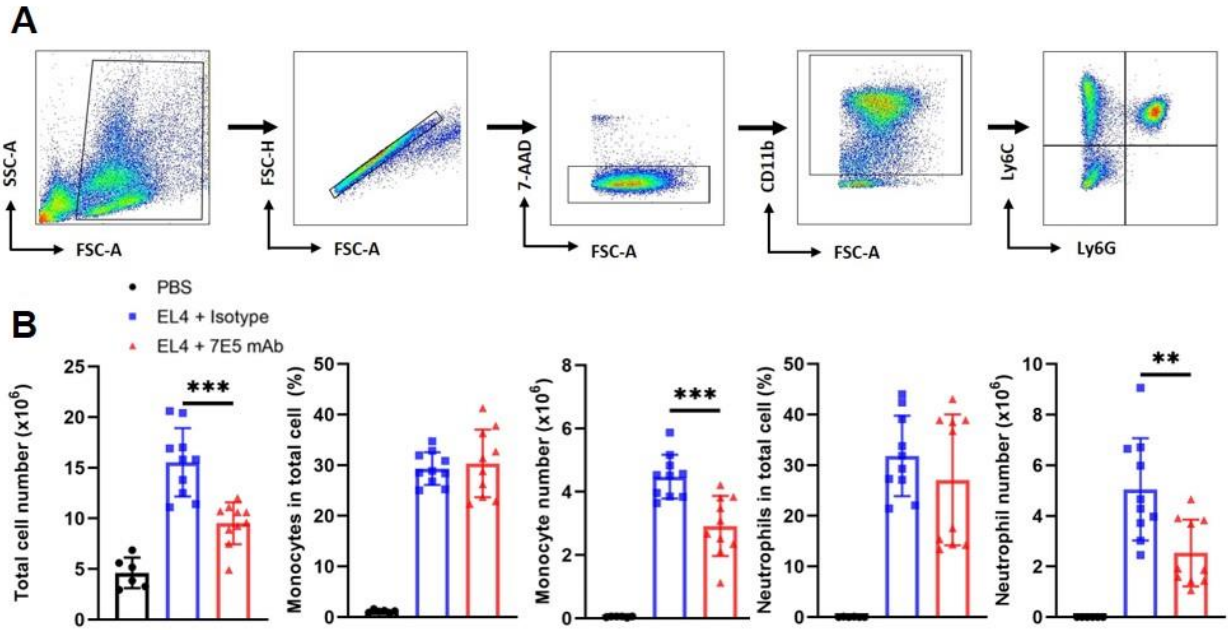

Figure 6. 7E5 mAb reduces inflammation stimulated by soluble ENO1

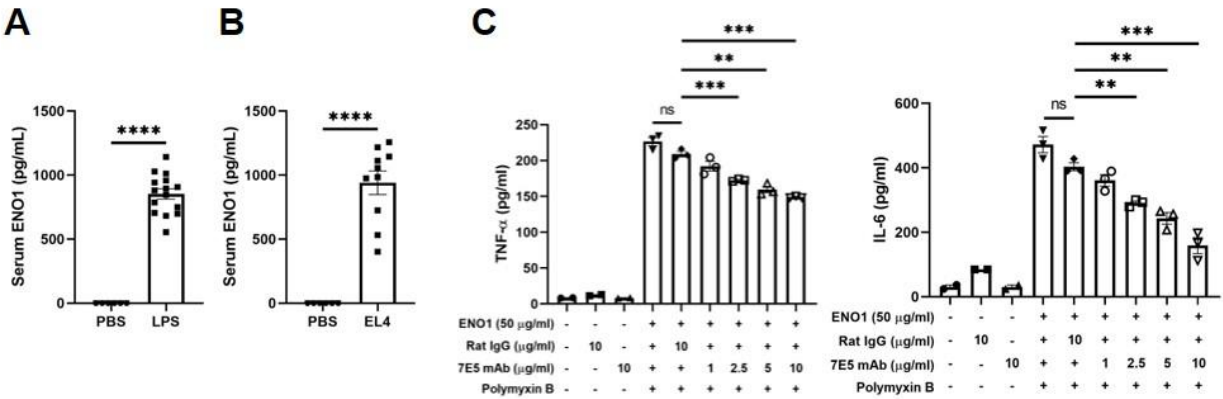
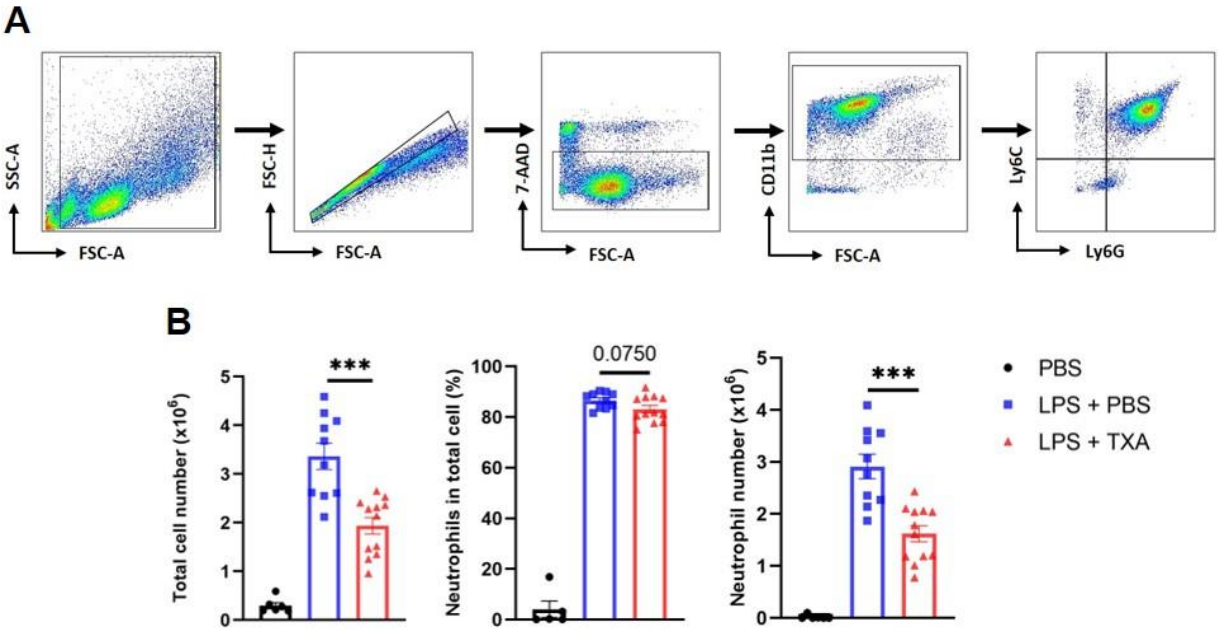
Figure 7. Neutrophil migration can be attenuated pharmacologically by a PLG inhibitor